



Mechanism of the selective reduction of NO_x by methane over Co-ZSM-5

Andrea Bellmann, Hanan Atia, Ursula Bentrup*, Angelika Brückner

Leibniz-Institut für Katalyse e. V. an der Universität Rostock (LIKAT), Albert-Einstein-Str. 29a, 18059 Rostock, Germany



ARTICLE INFO

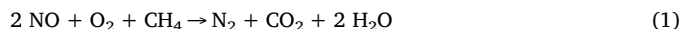
Keywords:
Co-ZSM-5
CH₄-SCR of NO_x
in situ spectroscopy
Operando DRIFTS/UV-vis

ABSTRACT

The selective catalytic reduction of NO_x by methane (CH₄-SCR) was studied on Co-ZSM-5 catalysts. Different Co-ZSM-5 and Co,Na-ZSM-5 catalysts were prepared by ion exchange, characterized by different methods, and were tested in CH₄-SCR. The catalytic performance depends on the Co content where catalysts with Co loadings between 2.5–3.0 wt.% showed the best. For mechanistic studies *operando* DRIFTS/UV-vis spectroscopy was employed enabling the simultaneous observation of surface adsorbates (DRIFTS), changes of Co oxidation state and coordination sphere (UV-vis), and product formation (MS). These measurements reveal that preadsorbed nitro/nitrito (NO_y) species formed by oxidation of NO at Co³⁺ species present in oxide-like clusters are reduced by gaseous CH₄ corresponding to an Eley-Rideal mechanism. Isocyanate species were identified as possible intermediates which react with the NO_y species or NO₂ to form N₂. This could also be confirmed by TG-DSC-MS investigation of Co-ZSM-5 impregnated with Na¹⁵NO₃ and NaOCN, where ¹⁵N¹⁴N was already formed at 288 °C in an exothermic reaction of ¹⁵NO₃[−] with OCN[−] catalyzed by Co because on a Co-free sample the ¹⁵N¹⁴N formation proceeds at significant higher temperature. The isolated Co²⁺ cations located at exchange positions play an indirect role, facilitating chemisorption of NO and, thus, practically act as storage sites for NO.

1. Introduction

While the selective catalytic reduction (SCR) of NO_x with NH₃ as reducing agent is a commercially applied technology for stationary and mobile sources such as diesel and lean-burn gasoline vehicles, the use of methane as reductant is an attractive technology to remove nitrogen oxides from oxygen-rich exhaust gases of stationary natural gas sources (Eq. (1)) [1,2].



As reported by Amor [1], in particular Co-ZSM-5 and Co-FER are very active in the catalytic reduction of NO_x by CH₄. Although numerous studies have been carried out in the past to understand the catalytic mode of action of this type of catalyst, the presented conclusions concerning the active sites, CH₄ activation, N₂ formation, and possible intermediates give a complex and sometimes inconsistent picture. Li and Amor [3] suggested that CH₄ could be activated through a Co-bound NO₂ species like NO₂[−] by forming CH₃ radicals and then CH₃NO₂ which further reacts with gaseous NO to form N₂. The involvement of methyl radicals was also discussed by Lukyanov et al. [4] as well as Sun et al. [5], while the latter authors assumed that hydrogen and methyl radicals could react with adsorbed NO₂ species generating CH₃NO₂ as intermediate.

Wang et al. [6] found that NO is oxidized and adsorbed as NO_y

species which react with CH₄, where isocyanate species were detected as possible intermediates. Experiments with ¹⁵NO revealed that the preadsorbed ¹⁴NO_y and isocyanate species give ¹⁴N¹⁵N species which suggests that one N atom comes from the deposit and one from gaseous NO or NO₂. Furthermore, the authors assumed a possible involving of Co⁰ clusters.

Cowan et al. [7] determined reaction rates using CH₄ and CD₄ containing feeds. From the observed kinetic effect they inferred that the breaking of the C–H bond is the rate-determining step. The kinetic isotope effect is slightly less for the selective reaction with NO than for the concurrent direct oxidation of CH₄. Hence, it was concluded that the rate-determining step involves detachment of hydrogen from methane by adsorbed NO₂ species to form a methyl species which further reacts with NO in one way and with oxygen in another.

Comprehensive studies using steady-state isotopic transient kinetic analysis (SSITKA) as well as characterization studies of Co-ZSM-5 with varying exchange degree were carried out to get mechanistic insight and for the identification of active species [8–10]. Thus, NO₂^{δ+} (formed on nanoclusters of cobalt oxide located inside the zeolite channels) as well as NO₂[−] species (formed on larger cobalt oxide particles located outside the zeolite channels) were identified as active intermediates formed by reaction of NO with molecularly adsorbed oxygen or oxidized surface sites [8]. These species directly react with methane forming NO_xCH_y intermediates which further react with NO and O₂ to

* Corresponding author.

E-mail address: ursula.bentrup@catalysis.de (U. Bentrup).

N_2 , CO_2 and water [9]. Three different Co species were discussed: (i) Co^{2+} cations located in the zeolite channels, (ii) microaggregates composed of cobalt and oxygen, and (iii) CoO and Co_3O_4 , including Co silicate for over-exchanged Co-ZSM-5 samples [10]. The microaggregates were found to be active in the CH_4 -SCR, while the larger Co oxide/silicate species were mainly involved in unselective parallel combustion reactions. The isolated Co cations play only an indirect role, allowing chemisorption of NO in form of nitrosyls and would act as storage sites.

That the CH_4 -SCR reaction over Co zeolite catalysts implies the activation of NO_x as adsorbed oxidized N_xO_y species that reacts with CH_4 from the gas phase or activated by adsorption into the zeolite channels was also supposed by other authors [11]. From additional spectroscopic characterization data they concluded that these strongly adsorbed N_xO_y intermediates are formed on oxidizing Co sites different from the most abundant Co^{2+} ions in exchange positions but located in the channels of the zeolite [12]. The involvement of active trivalent cobalt species located in the cavities of the zeolite but not in classical cation positions was also confirmed by TPR and FTIR spectroscopic studies on Co-H-MFI catalysts [13].

Hadjiiivanov et al. also found that in the simultaneous presence of NO and O_2 surface nitrates are the only stable species which easily react with methane or ethane, where organic nitro-compounds and isocyanates were detected as intermediate products [14]. With NO alone, stable $\text{Co}^{2+}(\text{NO})_2$ di-nitrosyls are formed which were assumed to be precursors for nitrate formation in the presence of oxygen [15].

Based on studies of CH_4 -SCR on Co-H-ZSM-5 and Co-H-mordenite Lónyi et al. [16] discussed a bifunctional mechanism, that means two catalytic functions are necessary for promoting (i) the NO_2 formation reaction and (ii) generating active surface NO_x intermediates which react in the SCR with methane. Thus, they claimed that the oxidation of NO to NO_2 proceeds over Brønsted acid sites and, if present, over Co-oxide species with significantly higher rate and provides intermediate $\text{NO}_3^-/\text{NO}^+$ species. These $\text{NO}_3^-/\text{NO}^+$ ion pairs then react with CH_4 under formation of N_2 , CO_2 and H_2O .

Kaucký et al. [17] studied the activity of different Co ion sites in ZSM-5, ferrierite, and mordenite in the CH_4 -SCR reaction. From the analysis of the Co(II) distribution on α , β , and γ cationic sites based on UV-vis spectroscopy [18–20] in combination with SCR activity studies [17] it was inferred that for Co-ferrierite and Co-mordenite the α -type Co ions were the most active sites, while for Co-MFI the most populated β -type Co ions were the most active ones. Furthermore, it was concluded that the location of Co ions in the inner zeolite volume, their coordination, and the distance between Co ions play an important role in their catalytic activity, but to which extent these individual factors determine the activity could not be answered.

With respect to the possible role of acidic protons in the CH_4 -SCR Campa et al. [21,22] described reverse effects for Co-ZSM-5 and Co-MOR catalysts. Because of the essential higher activity of H-ZSM-5 compared to Na-ZSM-5 it was concluded that the acidic protons might play a role, but, for Co-H-ZSM-5 and Co-Na-ZSM-5 the same activity was observed which argues against a role of these acidic protons in the presence of Co. Also for mordenites Brønsted acid sites have been found to be responsible for their CH_4 -SCR activity. However, the essentially more active catalysts Co-H-MOR and Co-Na-MOR with the same Co content and markedly different Brønsted acidity have the same activity which suggests that acid protons play a negligible role when Co is present.

The literature data can be summarized as follows. Different Co species exist (Co cations located in the zeolite channels, CoO_x microaggregates, and $\text{CoO}/\text{Co}_3\text{O}_4$, including Co silicate at the outer surface) the specific function of which is contrarily discussed. Furthermore, the possible involvement of Co^{3+} species is unclear. NO is oxidized and adsorbed as NO_y species (nitrate/nitrite or $\text{NO}_3^-/\text{NO}^+$ ion pairs) which react with CH_4 . Possible intermediates are CH_3NO_2 and isocyanate species which react with NO or nitrates to form N_2 and H_2O . The total

oxidation of CH_4 as side reaction is favored by CoO and Co_3O_4 .

Based on these controversially assumptions the present work aims to clarify (i) which are the active Co species, divalent or/and trivalent cobalt species, (ii) which are the active NO_y species, and (iii) which intermediate species are formed in the reaction of NO_y species with methane. Therefore, different Co-ZSM-5 and Co-Na-ZSM-5 samples were prepared by ion exchange, characterized by different methods, and catalytically tested in the CH_4 -SCR. For analyzing the nature of the formed Co species FTIR spectroscopy (adsorption of NO and CO), UV-vis spectroscopy, and H_2 -TPR was used. The acidic sites (Brønsted and Lewis acidity) were characterized by adsorption of pyridine. For mechanistic studies *operando* DRIFTS/UV-vis spectroscopy was used enabling the simultaneous observation of surface adsorbates (DRIFTS), changes of Co oxidation state and coordination sphere ((UV-vis)), and product formation (MS). For studying the reactivity of possible intermediates isotopic labeling experiments were additionally carried out.

2. Experimental

2.1. Catalyst preparation

The catalysts were prepared by ion exchange using aqueous solutions of $\text{Co}(\text{NO}_3)_2 \cdot 6 \text{H}_2\text{O}$ (Sigma Aldrich) or $\text{Co}(\text{CH}_3\text{COO})_2 \cdot 4 \text{H}_2\text{O}$ (Carl Roth). After heating 500 ml of the solution to 60 °C and pH adjusting to 6.9, 5 g of the zeolite $(\text{NH}_4)_2\text{ZSM-5}$ CBV 2314, Zeolyst International) was added and the suspension was stirred for 24 h. After filtration the sample was washed with 400 mL water per g zeolite and dried over night at 90 °C. Subsequently, the sample was calcined under a flow of synthetic air at 500 °C for 5 h. The Si/Al ratio (11.5) and the contents of Co, Al, and Na were determined by ICP-OES analysis (Table 1).

2.2. Catalytic activity

Catalytic measurements were performed in a microflow quartz reactor (6 mm i.d.) in the temperature range of 200–600 °C using a feed of 2000 ppm NO, 2000 ppm CH_4 , and 2% O_2 , balanced with He. The gas hourly space velocity (GHSV) was 70 000 h^{-1} (100 mg catalyst of 350–710 μm particle size, total flow of 100 ml min^{-1}). Before testing, each catalyst sample was pretreated in 2% O_2/He at 500 °C for 1 h.

For analyzing the gas composition at the exit of the reactor a (UV-vis)-Multigas Sensor (ABB) was used for NO and NO_2 , and an online gas chromatograph (Agilent) with TCD detector for N_2 , CH_4 , O_2 , CO (5 A column), and CO_2 , N_2O (PoraPlot Q column). The calculation of conversion and selectivity values is described in the supporting information.

2.3. Catalyst characterization

The temperature-programmed reduction measurements (H_2 -TPR) were performed in a Micrometrics Autochem II 2920 instrument. A

Table 1
Catalyst preparations, compositions and BET surface areas (SA).

Catalyst	SA m^2/g	Zeolite	c (Co salt)	Co	Na	Co/Al
0 Co	275	NH_4	0.00	0.00	0.00	0.00
2.84 Co	–	NH_4	0.05 Co nitrate	2.84	0.00	0.40
2.81 Co	264	NH_4	0.05 Co nitrate	2.81	0.00	0.40
0.32 Co	302	NH_4	0.0005 Co nitrate	0.32	0.00	0.04
4.89 Co	254	NH_4	0.05 Co acetate ^a	4.89	0.00	0.68
2.44 Co	–	NH_4	0.005 Co nitrate	2.44	0.00	0.30
1.5 Co, 1.08 Na	280	Na^b	0.05 Co nitrate	1.50	1.08	0.19
0.35 Co, 1.98 Na	–	0.8Na	0.0005 Co acetate	0.35	1.98	0.05
2.91 Co	–	0.8Na	0.05 Co nitrate ^a	2.91	0.00	0.43

^a Threefold ion exchange.

^b Na-ZSM-5 from Clariant (Si/Al = 13.5).

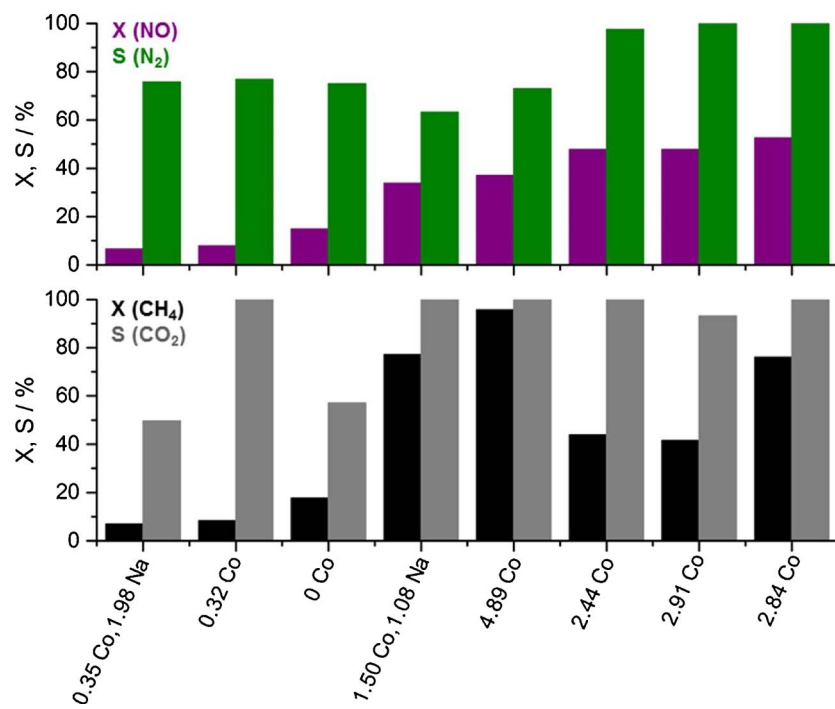


Fig. 1. Conversion of NO and CH₄ as well as selectivities of N₂ and CO₂ obtained for the different Co-ZSM-5 catalysts. Reaction conditions: 2000 ppm NO, 2000 ppm CH₄, 2% O₂, balanced with He, 100 ml/min, 500 °C, 70,000 h⁻¹.

100–250 mg sample was loaded in U shaped quartz reactor and heated in 5%O₂/He (50 ml/min) with 20 K/min up to 500 °C. After isothermal treatment at 500 °C for 60 min, the sample was cooled down to RT in a flow of Ar. The TPR run was carried out from RT to 1000 °C in a 5% H₂/Ar flow (20 ml/min) with a heating rate of 10 K/min. The hydrogen concentration was recorded by TCD detector in dependence on temperature. The hydrogen consumption was calculated by analyzing the respective peak areas of the TPR profile.

The UV-vis-DR spectra were recorded between 200 and 800 nm in diffuse reflection mode using a Cary 5000 spectrophotometer (Agilent) equipped with a diffuse reflection accessory (Praying mantis, Harrick). The spectra were measured at room temperature after a treatment in He at 400 °C for 30 min.

In situ FTIR measurements were carried out in transmission mode on a Thermo Scientific Nicolet 6700 spectrometer or iS10 spectrometer equipped with a custom-made reaction cells with CaF₂ windows for adsorption studies of NO, NO/O₂, pyridine (room temperature – 350 °C) and of CO (–120 to –60 °C), respectively, which were connected to a gas-dosing system and could be heated/cooled and evacuated. The sample powder was pressed into a self-supporting wafer with a diameter of 20 mm and a weight of 50 mg.

For each experiment the sample was pretreated by heating in synthetic air (50 ml/min) up to 400 °C. After cooling and flushing with He at reaction temperature (room temperature or 350 °C) for 20 min, the sample was exposed to the different gas mixtures (2000 ppm NO/He; 2000 ppm NO/2% O₂/He; 5%CO/He) using a total gas flow of 50 ml/min. More details of experiment procedures are given in the respective chapters of the following section. Generally, the spectrum of the catalyst measured after pretreatment at reaction temperature was subtracted from the respective adsorbate spectra.

Simultaneous TG-DSC-MS measurements were performed on a Sensys TG-DSC (Setaram) connected to an OmniStar quadrupole mass spectrometer (Pfeiffer Vacuum). The samples (20 mg) were heated in He (20 ml/min) up to 600 °C with a heating rate of 2 K min⁻¹. For these experiments 100 mg of the catalyst samples 0 Co and 2.81 Co were impregnated by incipient wetness method, respectively, using a solution of 20 mg Na¹⁵NO₃ and 20 mg NaOCN in 1 ml H₂O. After

impregnation the samples were dried at 90 °C for 24 h.

2.4. Operando DRIFTS/UV-vis measurements

The DRIFTS (Diffuse Reflection Infrared Fourier Transform Spectroscopy) measurements were carried out on a Nicolet 6700 spectrometer (Thermo Scientific) equipped with a commercial reaction cell (Harrick) with CaF₂ windows connected to a gas-dosing system. The reaction cell was modified (Fig. SI-1) using the quartz observation window in the dome to implement a custom-built high-temperature reflection probe (Avantes). The latter contacts the solid catalyst sample directly without disturbing the optical path of the IR beam. For analyzing the products the gas outlet of the reaction cell was connected to an OmniStar quadrupole mass-spectrometer (Pfeiffer Vacuum). Generally, the samples (particle size: 710 – 350 µm) were pretreated by heating in 2% O₂/He at 400 °C for 90 min. Then, the samples were exposed to different gas mixtures (cf. 3.3.2.) at 350 °C containing 2000 ppm NO, 2000 ppm CH₄, 2% O₂, and 0.1% Ne as internal standard for the MS balanced with He with a total flow of 32 ml/min.

To perform experiments with labelled ¹³CH₄ an electric four way valve (VICI) was installed to realize a quick switch between ¹²CH₄/NO/O₂ and ¹³CH₄/NO/O₂ feed maintaining a constant flow rate of 32 ml/min. After the above mentioned pretreatment (90 min heating in 2% O₂/He at 400 °C) the sample was exposed to the unlabeled feed. After reaching steady-state [23] it was switched from the normal non-labeled gas mixture (4000 ppm NO, 5000 ppm ¹²CH₄, 2% O₂, and 0.1% Ne balanced with He) to the respective labeled feed (4000 ppm NO, 1% ¹³CH₄, 2% O₂, and 0.1% Ne balanced with He).

3. Results and discussion

3.1. Catalytic performance

The conversions of NO and CH₄ as well as the selectivities of N₂ and CO₂ obtained for the different catalysts (cf. Table 1) at 500 °C are presented in Fig. 1. Because no C–N products were detected the selectivities could be determined element-specifically. The formation of

N_2O was not observed for any catalyst. At some catalysts NO_2 and CO were observed as byproducts (Fig. SI-2).

The catalytic performance depends on the Co content where Co concentrations between 2.5–3.0 wt.% seem to be optimal. Surprisingly, the catalysts with low Co content (e.g. 0.32 Co) show a worse performance compared to the 0 Co catalyst. This points to the fact that Brønsted acidic hydroxyls the concentration of which is higher in the 0 Co (*vide infra*) participate in the reaction more effectively than the Co species. On the other hand, iron impurities as detected by NO adsorption on 0 Co (*vide infra*) can contribute to catalytic activity.

The CH_4 conversion depends on the Co content, too. Here, it is interesting that the 1.50 Co, 1.08 Na catalyst with lower Co content shows similar activity compared to the high loaded 4.89 Co catalyst. It seems that the catalytic performance is strongly related to the nature of Co species existing in the respective catalyst. Therefore, the variety of Co species as well as surface acidity of selected catalysts were characterized by different methods.

3.2. Catalyst characterization

3.2.1. Acidity -adsorption of pyridine

Pyridine is a suitable basic probe molecule to characterize both Brønsted and Lewis acidic sites by FTIR spectroscopy [24,25]. The typical band of pyridine fixed to Brønsted acid sites (PyH^+) is observed at around 1540 cm^{-1} . Bands resulting from pyridine interacting with Lewis acid sites (L-Py) are observable at around 1450 cm^{-1} and in the region 1625 – 1595 cm^{-1} . From the band position in the latter region the strength of Lewis acid sites can be evaluated [25]. The pyridine adsorbate spectra of selected catalysts are depicted in Fig. 2. The spectra were recorded at $200\text{ }^\circ\text{C}$ to exclude an overlap of the bands of L-Py and hydrogen bonded pyridine (hb-Py). As expected, the Co-free sample shows an intense PyH^+ band at 1544 cm^{-1} the intensity of which decreases with Co loading. Comparing the band intensities of the PyH^+ band it is obvious that even the high loaded samples (2.81 Co, 4.89 Co) possess a comparable high amount of Brønsted acid sites which is different as expected from the Co/Al ratio but in accordance with observations of other authors [22]. They also report about unexpected Brønsted acidic sites in Co-MOR and concluded that the exchange process had a more complex stoichiometry. This is also true for Na-ZSM-5 where it is difficult to obtain samples with no protonic sites due to probable equilibrium between protons in the water and Na cations [26]. We also observed in the case of 1.50 Co, 1.08 Na that a high amount of Na from the Na-ZSM-5 (2.26 wt.% Na) which was used for

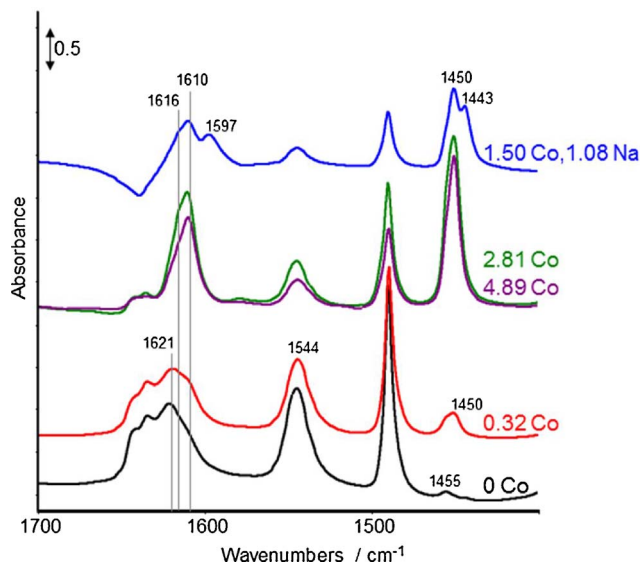


Fig. 2. Pyridine adsorbate spectra of different catalysts measured at $200\text{ }^\circ\text{C}$.

ion exchange have been lost.

With increasing Co content additional Lewis acid sites are created indicated by bands at 1450 / 1610 cm^{-1} (Co^{2+}) and 1443 / 1597 cm^{-1} (Na^+). The band at 1621 cm^{-1} stems from pyridine adsorbed on Al^{3+} sites [25]. By careful inspection of the region above 1600 cm^{-1} , a splitting of the L-Py band into two components with band positions at 1610 and 1616 cm^{-1} can be observed revealing two Co^{2+} Lewis sites of different strength possibly located at different sites in the zeolite lattice.

3.2.2. Adsorption of CO and NO

For characterizing the nature of the different Co species the adsorption of CO at low temperatures is an appropriate method. Comprehensive studies of Góra-Marek et al. [27–29] revealed that Co^{2+} located at exchange positions and Co^{2+} occurred in form of oxide-like clusters can be distinguish by CO adsorption at low temperature ($-100\text{ }^\circ\text{C}$). Thus, Co^{2+} located at exchange positions is characterized by a Co^{2+} –CO band at 2204 cm^{-1} while Co^{2+} in oxide-like clusters shows a carbonyl band at 2194 cm^{-1} . Because Co^{3+} species do not form carbonyls they can be easily detected by NO adsorption at room temperature [28]. By preadsorption of molecules that are not able to penetrate the channels of zeolites like ZSM-5 or MOR, it is possible to distinguish between cationic sites inside and outside the channels and, therefore, to characterize the sites on the external surface [12,13,30]. Thus, it could be shown by the combination of CO and NO adsorption after preadsorption of o-toluenonitrile on Co-H-MFI that Co^{3+} species are located inside the zeolite channels while Co^{2+} ions are distributed both, at the external and internal surfaces [13].

We have studied both, the low temperature adsorption of CO and the room temperature adsorption of NO. Generally, the CO adsorption was carried out at $-120\text{ }^\circ\text{C}$, and then the temperature- programmed desorption under vacuum was followed (Fig. 3a). While the bands at 2205 and 2194 cm^{-1} are assigned to Co^{2+} –CO vibrations, the band at 2174 cm^{-1} results from the interaction of CO with OH groups [31]. The latter band vanishes at higher temperatures because the interaction of CO with hydroxyl groups is not as strong as the interaction with Co^{2+} ions. Therefore, the CO adsorbate spectra at $-60\text{ }^\circ\text{C}$ for selected samples are compared in Fig. 3b to inspect the Co^{2+} –CO vibrations properly. Considering that the bands at 2205 and 2194 cm^{-1} reflect Co^{2+} –CO vibrations of Co^{2+} located at exchange positions and in oxide-like clusters, respectively, it is obvious that all Co samples contain Co^{2+} species at exchange positions as well as in oxide-like clusters independent from the Co content and despite the high Co/Al ratio of e.g. 2.81 Co and 2.44 Co (cf. Table 1). Even in the 0.32 Co sample only a part of the Co^{2+} ions is located at exchange positions. In the Na-containing sample (1.50 Co, 1.08 Na) practically all Co^{2+} is present in oxide-like clusters (band at 2190 cm^{-1}). The band at 2178 cm^{-1} can be assigned to Na^+ –CO vibrations [32].

For inspecting possible Co^{3+} species the NO adsorption at room temperature was used. Because a reduction of Co^{3+} species by NO already at room temperature cannot be excluded a short adsorption time (max. 30 min) or low NO concentrations have to be applied [28].

The NO adsorbate spectra of selected catalysts recorded after 17.5 min exposure time to NO (200 ppm NO/He) are shown in Fig. 4a. This point was selected because a constant intensity of the band at 1941 cm^{-1} was reached (Fig. 4b). This band corresponds to Co^{3+} –NO linear species, where the bands at 1812 / 1896 cm^{-1} are characteristic for Co^{2+} –(NO)₂ dinitrosyls [33]. For the catalyst 0 Co two bands at 1893 and 1878 cm^{-1} are observable which obviously stem from two kinds of Fe^{2+} –NO linear species [34], because ZSM-5 contains low concentrations of iron. In general, the band intensities of Co^{3+} –NO and Co^{2+} –(NO)₂ go along with the Co concentrations. However, a comparable high concentration of Co^{3+} was detected in the sample 1.50 Co, 1.08 Na compared to 2.81 Co (Fig. 4b). This can be related to the appearance of mainly oxide-like clusters in the pores (cf. Fig. 3b) in which Co^{2+} can be easily oxidized to Co^{3+} during the oxidative pretreatment. Surprisingly, a continuous increase of the 1812 cm^{-1} band intensity

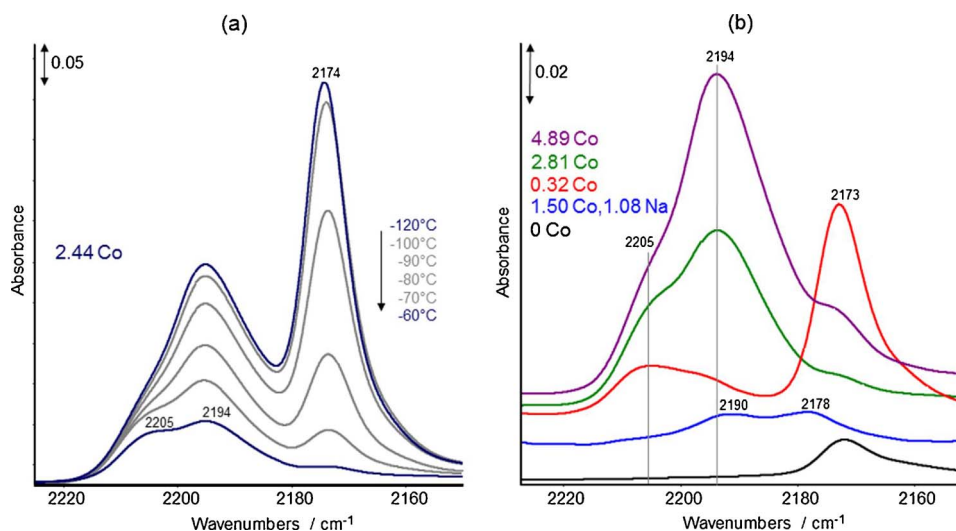


Fig. 3. CO adsorbate spectra of 2.44 Co in dependence on temperature (a) and comparison of the CO adsorbate spectra of selected catalysts measured at -60 °C (b).

indicating Co²⁺ is observed, although in principle no intensity drop of the Co³⁺-NO band (1941 cm⁻¹) is seen. Moreover, the time-dependent band intensity evolution of the catalysts 1.50 Co, 1.08 Na and 4.89 Co is very similar (Fig. 4b) despite the distinct differences of the Co content.

This suggests the presence of additional Co³⁺ containing oxide species most probably located at the outer surface which are partly reduced by NO forming additional accessible Co²⁺ sites. Interestingly, in parallel to the bands at 1812/1896 cm⁻¹, a band around 1638 cm⁻¹ (Fig SI-3) is rising during NO exposure which points to the simultaneous formation of NO₂ [35].

3.2.3. UV-vis-DRS and TPR

The presence of a comparable high amount of Co³⁺ in the catalyst 1.50 Co, 1.08 Na is also reflected by the UV-vis spectrum (Fig. 5). While for the 2.81 Co catalyst a triplet of bands is seen being characteristically for Co²⁺ in tetrahedral surrounding [10,36], the spectrum of 1.50 Co, 1.08 Na is rather dominated by an intense band around 345 nm. This band is attributed to a ligand to metal charge transfer transition from framework oxide ions to Co³⁺ ions [36,37] and is also seen in the spectrum of 2.81 Co, but to a lower extend. Both features of Co²⁺ and Co³⁺ species are also observable in the 4.89 Co sample, but due to the high cobalt content the UV-vis spectrum is not well resolved.

Further information concerning the nature of Co species are available from H₂-TPR studies. The TPR profiles of selected catalysts are depicted in Fig. 6 and comprise three temperature regions: i) 200–350 °C, ii) 600–900 °C, and iii) above 900 °C, whereas the last peak is not complete and only the beginning of H₂ consumption is observable. The peaks at 220/300 °C result from the reduction of Co₃O₄ [38,39], and are clearly seen at the sample 4.89 Co with the highest Co content, but for the sample 1.50 Co, 1.08 Na to a lower extent, too. This finding is in accordance with the results of the NO adsorption experiments (cf. Fig. 4b) and the UV-vis data (cf. Fig. 5) and confirms the similar characteristics of both samples, despite from the different Co content. The peaks between 600–900 °C are differently interpreted, thus, assigned to the reduction of Co cations in exchange position and/or reduction of (CoO)_x oxide clusters in the channels of the zeolite [38]. On the other hand, Mhamdi et al. [40] reported that Co-ZSM-5 catalysts prepared from cobalt acetate show a distinct TPR peak between 740 and 780 °C, and it could be proved that this peak results from the reduction of Co ions in phyllosilicate phases at the surface of zeolite grains. Because the 4.89 Co catalyst was prepared with Co acetate, too, the strong TPR peak at 700 °C (Fig. 6) is assigned to the reduction of Co ions in phyllosilicate phases. The formation of such phyllosilicate phases was also verified by TEM investigations (Fig. SI-4). Because the 1.50 Co, 1.08 Na catalyst shows a TPR peak at comparable temperature

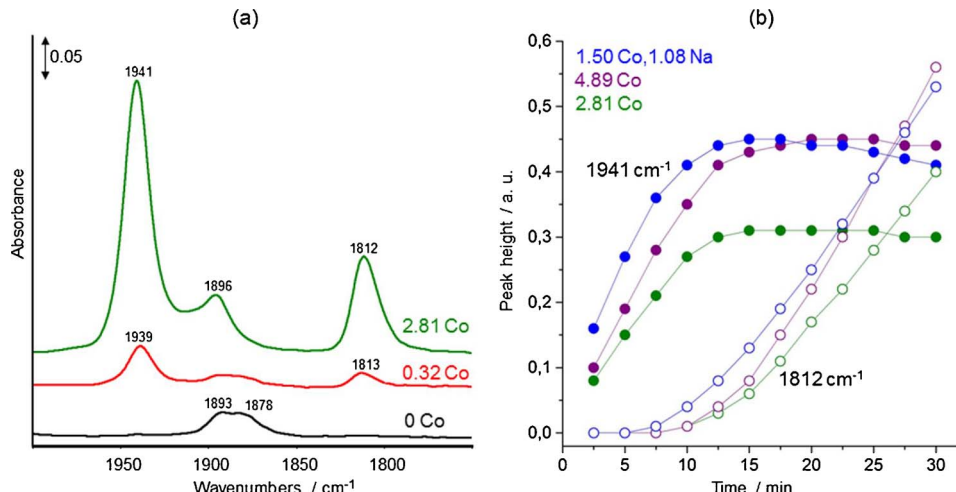


Fig. 4. NO adsorbate spectra of selected catalysts measured after 17.5 min exposure time at room temperature (a) and band intensities (1941 and 1812 cm⁻¹) measured on selected catalysts in dependence on exposure time to NO (b).

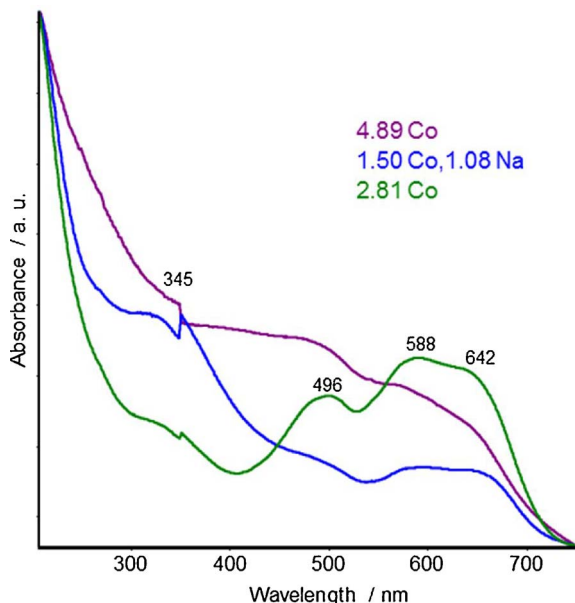


Fig. 5. UV-vis spectra measured in diffuse reflection mode at room temperature after heating the samples at 400 °C in He for 30 min.

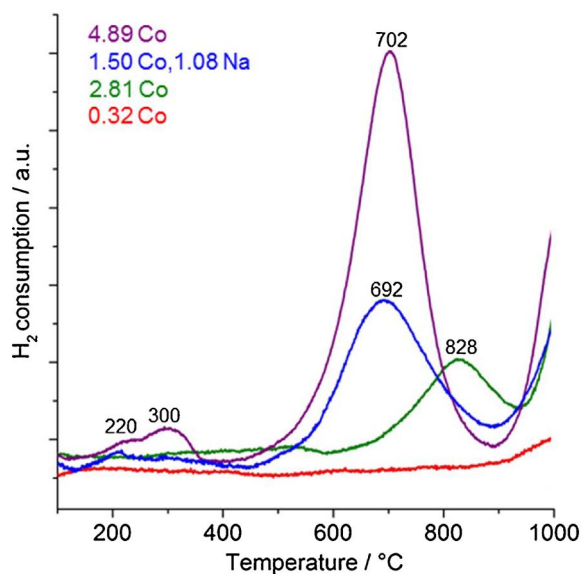


Fig. 6. H₂-TPR profiles of selected catalysts.

(692 °C), this peak is also assigned to the reduction of Co ions in phyllosilicate phases. It seems that in the presence of Na ions the formation of Co oxide and phyllosilicate species is favored.

The 2.84 Co catalyst shows a peak around 830 °C which can be attributed to the reduction of Co²⁺ in oxide-like clusters the presence of which was confirmed by CO adsorption experiments (cf. Fig. 3b). In all TPR profiles a further starting H₂ consumption peak is seen at temperatures above 900 °C, the slope of which differs depending on Co content. We suggest, in contrast to the assignments given in literature [38,39], that this slope indicates the beginning reduction of Co²⁺ in exchange positions.

Looking at data of consumed H₂ calculated from the TPR peaks for each sample (Table 2) it is obvious that some of the Co ions remain unreduced, because the amount of consumed H₂ should be equivalent to the amount of Co²⁺ per gram catalyst assuming that all Co²⁺ is reduced. Moreover, if Co³⁺ is present the amount of consumed H₂ should be higher, but this is not the case. This finding is in agreement

Table 2
H₂-TPR results of selected catalysts.

Catalyst sample	Co content wt.%	Co content μmol/g	H ₂ consumption μmol/g	Percentage of reduced Co
2.84Co	2.84	482	289	60%
4.89Co	4.89	830	749	90%
1.50Co,1.08Na	1.50	254	225	89%
0.32Co	0.32	54	14	26%

with observations described also by other authors [38,39,41] and supports our assumption that a certain percentage of Co²⁺ ions most likely present in exchange positions is reduced only above 900 °C.

Summing up the findings of the characterization experiments the following can be stated: i) independently from the Co content only a part of Co²⁺ is located at exchange positions because Brønsted acidic sites were detected at all catalysts; ii) Co²⁺ is located at exchange positions as well as in oxide-like clusters; iii) all catalysts contain a remarkable percentage of Co³⁺ which is formed by calcination in air and is present in Co₃O₄ as well as in oxide-like clusters and/or phyllosilicate phases.

3.3. Mechanistic studies

3.3.1. Interaction of the catalyst with the feed components CH₄, NO and NO/O₂

Generally, the mechanistic studies were carried out at 350 °C, a temperature at which the active catalysts show appropriate NO and CH₄ conversions. By exposing the most active catalyst 2.84 Co pretreated in 2% O₂/He with CH₄ alone, no adsorbates were detected by DRIFTS and no changes were observed in the UV-vis spectrum. This is not surprising because TPR studies with 10% CH₄/He showed (Fig. SI-5) that CH₄ reduces the 4.89 Co catalyst at 675 °C and the 2.81 Co catalyst only at 725 °C. Consequently, CH₄ is not activated and is not able to reduce the catalyst at the reaction temperature of 350 °C.

The transmission spectra obtained after interaction of 2.81 Co with firstly NO, secondly O₂ and thirdly NO/O₂ at 350 °C are displayed in Fig. 7. Here, the IR cell was first flushed with the reactant stream for 10 min (flowing conditions), and then the cell was closed (static conditions) and spectra were recorded in dependence on time.

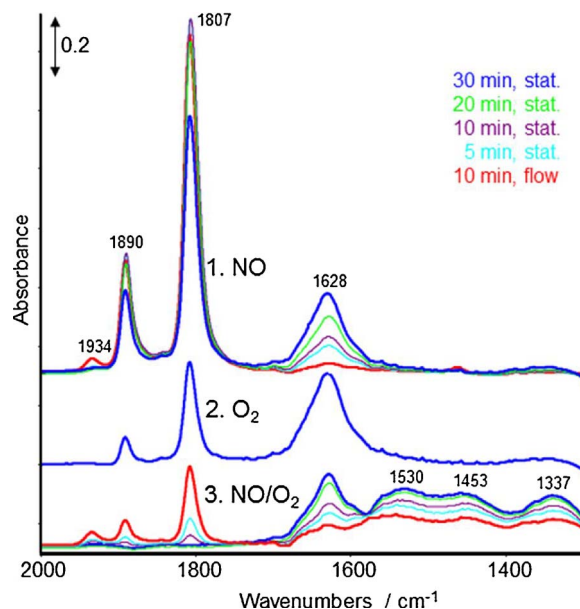


Fig. 7. Adsorbate spectra of 2.81 Co obtained during consecutive exposure to 1. NO/He, 2. O₂/He, and 3. NO/O₂/He at 350 °C after flowing conditions for 10 min and static conditions for 30 min, respectively.

During NO adsorption the typical bands of Co^{3+} –NO linear species (1934 cm^{-1}) and Co^{2+} –(NO)₂ dinitrosyls ($1812/1896\text{ cm}^{-1}$) can be seen (cf. Fig. 4), while the intensity of the Co^{3+} –NO band is comparably low and rapidly drops under static conditions. Simultaneously, a new band rises at 1628 cm^{-1} which is related to NO_2 [35] most probably adsorbed at Co^{2+} sites. The appearance of a negative band around 3602 cm^{-1} (Fig. SI-6) indicates an interaction of the formed NO_2 with acidic hydroxyl groups.

The oxygen needed for NO_2 formation is obviously supplied by Co^{3+} -containing oxide species which are reduced by NO. Subsequent exposure to O_2/He causes partly removing of NO but does not change the intensity of the NO_2 band. That means that Co^{3+} is rapidly reduced by NO while additional O_2 is not able to further oxidize NO_2 as well as adsorbed NO at this temperature.

During adsorption of NO/O_2 new bands appear around $1530/1337\text{ cm}^{-1}$ and 1453 cm^{-1} which can be assigned to bidentate nitro and monodentate nitrito species (NO_y species), respectively [35]. While the intensity of these bands grows up with time, the Co^{3+} –NO and Co^{2+} –(NO)₂ bands vanish completely indicating a continuous oxidation of NO to NO_2 and NO_y species under static conditions.

These experiments lead to the conclusion that NO_y species are only formed in NO/O_2 feed, and Co^{3+} species present in oxide-like clusters present in the zeolite pores are needed for the oxidation of NO and NO_2 . Furthermore, it can be assumed that gaseous oxygen is required to re-oxidize the formed Co^{2+} under flowing conditions and, thus, to create an active Co^{3+} – Co^{2+} redox pair.

This conclusion is in accordance with other findings inferring that the active sites for CH_4 -SCR in Co-ZSM-5 are trivalent Co species located in the cavities and are able to convert NO to an adsorbed higher oxidation state NO_y species, possibly bridging nitrate species [13]. That means, in turn, as also assumed by Chupin et al. [10] and Montanari et al. [12], that isolated Co cations cannot be considered active sites. They rather play an indirect role, allowing chemisorption of NO and, thus, act as storage sites for NO.

3.3.2. Interaction of preadsorbed NO_y species with CH_4 : operando DRIFTS/UV-vis-DRS

To study the reactivity of preadsorbed NO_y species against CH_4 *operando* DRIFTS/UV-vis measurements were carried out exemplarily on the 2.81 Co catalyst enabling the simultaneous monitoring of adsorbate formation on the catalyst surface by DRIFTS, changes of redox behavior and coordination of Co species by UV-vis-DRS and product formation by MS.

The DRIFT spectra obtained after NO/O_2 adsorption at $350\text{ }^\circ\text{C}$ and He flushing as well as after subsequent dosing of CH_4 are shown in Fig. 8a (spectral region 2325 – 1300 cm^{-1}) and Fig. 8b (spectral region 3800 – 3500 cm^{-1}). After NO/O_2 adsorption bands of adsorbed NO_y species are seen at $1562/1306\text{ cm}^{-1}$ and 1479 cm^{-1} assigned to bidentate nitro and monodentate nitrito species, respectively. Due to the method-related specifics (DRIFTS provides rather information from the surface, while in transmission mode the whole volume is inspected) [42,43] band positions and relative intensities are slightly different from those showed in Fig. 7. During dosing of CH_4 the intensity of the NO_y bands decreases and a new band at 1626 cm^{-1} appears the intensity of which rises continuously (Fig. 8a). At the same time in the OH region a new band at 3657 cm^{-1} grows up (Fig. 8b). Both bands are related to the formation of water and points to the reduction of NO_y species by CH_4 . Bands at 1582 and around 1306 cm^{-1} remain belonging to obviously not reactive bidentate nitro species. With starting exposure to CH_4 new bands appear at 2268 and 2182 cm^{-1} where particularly the intensity of the band at 2268 cm^{-1} decreases distinctly with exposure time and new bands with lower intensity appear at 2316 and 2284 cm^{-1} .

It is known from studies of HNCO adsorption [44] and CH_3NO_2 decomposition over Co-ZSM-5 and Cu-ZSM-5 [45–48] that the asymmetric stretch of Al^{3+} –NCO is expected in the range of

2260 – 2273 cm^{-1} and that of Co^{2+} –NCO between 2170 – 2196 cm^{-1} . Furthermore, it was found by adsorbing HNCO on pure ZSM-5 samples with different Si/Al ratios that two bands at 2260 and 2300 cm^{-1} were detectable which are related to Al^{3+} –NCO and Si^{4+} –NCO, respectively [44]. According to these literature data the observed bands at 2268 and 2182 cm^{-1} (Fig. 8a) are assigned to the asymmetric stretch of Al^{3+} –NCO and Co^{2+} –NCO, respectively, where the band at 2316 cm^{-1} obviously stems from Si^{4+} –NCO. The intensity of the Al^{3+} –NCO band changes markedly during the first 10 min of CH_4 exposure and shifts from 2268 to 2278 cm^{-1} and finally after 30 min to 2284 cm^{-1} . While the intensity drop can be explained by a possible high reactivity of these species, the shift might be caused by the accompanied water formation and subsequent creating of acidic hydroxyl groups at these Al^{3+} sites indicated by the band at 3657 cm^{-1} (Fig. 8b). Nitromethane and isocyanate species are discussed as possible intermediates in CH_4 -SCR. Thus, the question arises what role the isocyanate species play (*vide infra*).

Looking at the simultaneously recorded MS data (Fig. 8c) it can be seen that N_2 as well as CO_2 are immediately formed after CH_4 dosing. This indicates that the formation of N_2 is induced by the reduction of NO_y species with CH_4 . Interestingly, also NO_2 is detectable the formation of which might be caused by partly decomposition of instable NO_y species in the CH_4 flow [51].

In Fig. 8d selected UV-vis spectra are displayed which were simultaneously measured after oxidative pretreatment, after NO/O_2 preadsorption and He flushing, and after subsequent exposure to CH_4 and He flushing. After oxidative pretreatment the typical bands for Co^{2+} in tetrahedral surrounding (495, 585, 645 nm) and the $\text{O}^{2-} \rightarrow \text{Co}^{3+}$ LMCT band around 350 nm are seen. During preadsorption of NO/O_2 the intensity of the latter band decreases while the intensities of the typical bands for Co^{2+} increase. This indicates the reduction of Co^{3+} present in Co_3O_4 and oxide-like clusters as result of NO and NO_2 oxidation leading to a higher percentage of Co^{2+} . During exposure to CH_4 no more change of the Co^{2+} band is observable, which indicates no reduction of Co^{3+} by CH_4 . However, the intensity of the band around 350 nm further declines. It is known that adsorbed nitrate species increase the overall absorption in the CT region as described for $\text{Co}/\text{Al}_2\text{O}_3$ catalysts [52,53]. Thus, ionic nitrate shows an absorption maximum around 300 nm . Therefore, the decreasing intensity of the band around 350 nm is attributable to the reduction and therefore removing of NO_y species by CH_4 .

Summarizing the findings of the *operando* DRIFTS/UV-vis measurements it can be stated that preadsorbed NO_y species formed by oxidation of NO at Co^{3+} sites are reduced by gaseous CH_4 corresponding to an Eley-Rideal mechanism. As a consequence of this reaction N_2 is formed accompanied by water and CO_2 formation while isocyanate species were detected as possible intermediates.

This is in accordance with findings of Chupin et al. [10] and Montanari et al. [12,13] who found that Co oxide-like micro aggregates containing Co^{3+} and Co^{2+} [10] and/or Co^{3+} species located in the cavities but likely in non-classical cation position [13] are responsible for NO oxidation to higher oxidation state NO_y species. We could firstly show by simultaneous *operando* DRIFTS/UV-vis measurements that the formation of NO_y species (DRIFTS), which requires oxidizing sites, is accompanied by the reduction of Co^{3+} and consequently formation of Co^{2+} the higher percentage of which was observed by (UV-vis). The adsorbed NO_y species are reduced by CH_4 forming isocyanate species as intermediates (DRIFTS) which then react with NO or NO_2 to N_2 , CO_2 and H_2O as also found by Montanari et al. [13].

Because other authors mainly discussed catalytic activity in relation to the existing Co^{2+} species (e.g. Refs. [16,17,21,22]) the crucial role of Co^{3+} species in the CH_4 -SCR has been underestimated. Only not further specified Co oxide clusters and Co_3O_4 [17,38], detected in over-exchanged samples, have been identified to enhance oxidation of NO to NO_2 .

Generally it can be said that only by applying preferably

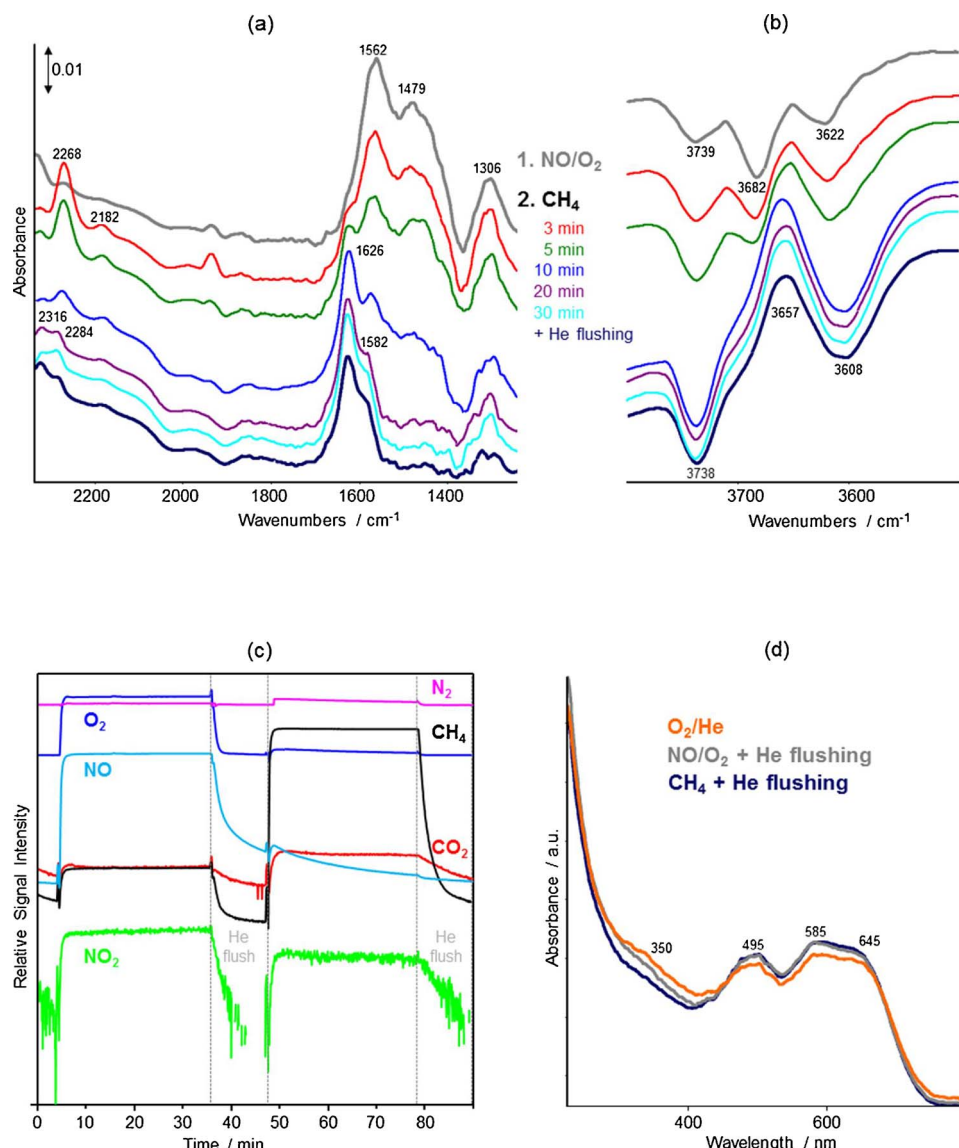


Fig. 8. Operando DRIFTS/(UV-vis)-DRS experiment: DRIFT spectra measured after $\text{NO}/\text{O}_2/\text{He}$ adsorption on 2.81 Co catalyst at 350 °C for 30 min and He flushing and subsequent exposure to CH_4/He in the spectral region $2330\text{--}1250\text{ cm}^{-1}$ (a) and $3775\text{--}3500\text{ cm}^{-1}$ (b), simultaneously recorded MS profiles (c), and UV-vis spectra measured after oxidative pretreatment, after $\text{NO}/\text{O}_2/\text{He}$ preadsorption and He flushing and after subsequent exposure to CH_4/He and He flushing (d).

simultaneous combination of complementary methods a comprehensive characterization of the Co species is ensured, on the basis of which the active species can be identified.

3.3.3. Role of isocyanate species and their reaction with NO_y species

To unravel the role of isocyanate species isotopic transient experiments were carried out. For this purpose it was switched from the $^{12}\text{CH}_4/\text{NO}/\text{O}_2$ feed after reaching steady state to the $^{13}\text{CH}_4/\text{NO}/\text{O}_2$ feed. By comparing the isotopic exchange rates of the surface isocyanate species, monitored by DRIFTS and gas phase species measured by MS, it is possible to discriminate between active and spectator species [54]. The DRIFT spectra and MS profiles measured during the switching experiment are displayed in Fig. 9.

By switching from the unlabeled to the labeled feed the $\text{Al}^{3+}\text{--N}^{12}\text{CO}$ band intensity drops quickly and a new one appears around 2209 cm^{-1} the intensity of which increases with time (Fig. 9a). The observed isotopic shift of 60 cm^{-1} correlates with the expected one if $^{12}\text{C}/^{13}\text{C}$ participates in the vibration [35]. Therefore this band is assigned to the respective $\text{Al}^{3+}\text{--N}^{13}\text{CO}$ vibration. Comparing the MS profiles of $^{13}\text{CH}_4$ and $^{13}\text{CO}_2$ (Fig. 9b) it is obvious that the formation of

$^{13}\text{CO}_2$ is delayed and proceeds slower as the $\text{Al}^{3+}\text{--NCO}$ band vanishes. This suggests that the isocyanate species are active intermediates [54].

Based on this finding the question remains in which way N_2 is formed. Taking into account that the isocyanate nitrogen has the oxidation state -3 , oxidizing nitrogen-containing agents like nitrates are needed to form N_2 . Because it is difficult to prove a possible reaction of isocyanate species with adsorbed nitrate species spectroscopically, we have studied this probable reaction by simultaneous thermal analysis coupled with MS detection of the evolved gases (TG-DSC-MS). Therefore, the 2.81 Co and 0 Co catalysts were impregnated with $\text{Na}^{15}\text{NO}_3$ and NaOON to mimic adsorbed NO_y and isocyanate species which are also present at the catalyst surface when the catalyst with preadsorbed NO_y species is exposed to CH_4 . These samples were heated in He with $2\text{ K}/\text{min}$, and the TG and DSC curves as well as the MS profiles of possible products were recorded. In Fig. 10 the TG and DSC curves as well as the MS profiles of exemplarily $^{15}\text{N}^{14}\text{N}$ ($m/z = 29$)/ ^{15}N ($m/z = 15$), H_2O ($m/z = 18$), and $^{15}\text{NO}_2$ ($m/z = 47$) are shown for the impregnated 2.81 Co and 0 Co catalysts.

The TG curve of the impregnated 2.81 Co catalyst (Fig. 10a) shows a step between $50\text{--}225\text{ }^\circ\text{C}$ which is accompanied by an endothermic effect

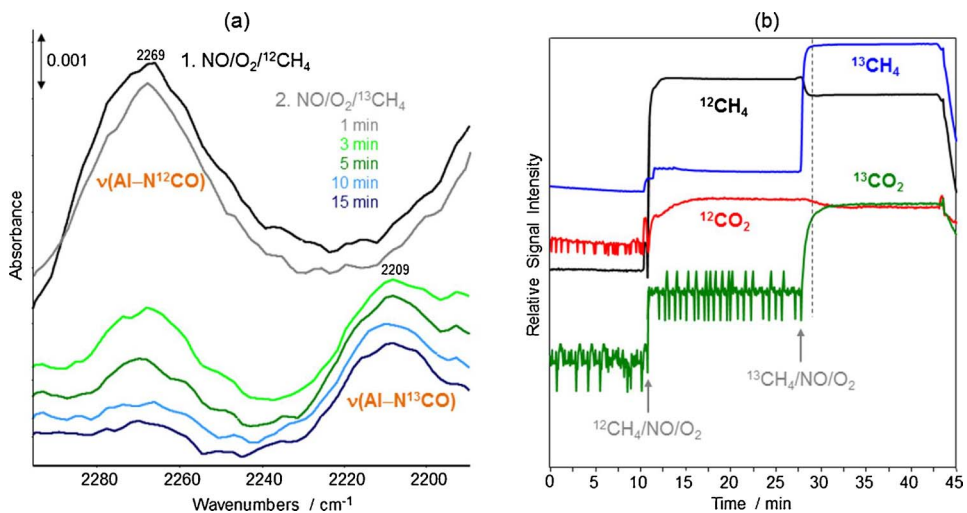


Fig. 9. DRIFT spectra of 2.84 Co catalyst measured after 15 min exposure to 4000 ppm NO/5000 ppm ¹²CH₄/2% O₂/0.1% Ne/He and after switching to the respective labeled feed (4000 ppm NO/1% ¹³CH₄/2% O₂, /0.1% Ne/He at 350 °C (a) and the simultaneously recorded MS profiles of ¹²CH₄/¹³CH₄ and ¹²CO₂/¹³CO₂ (b).

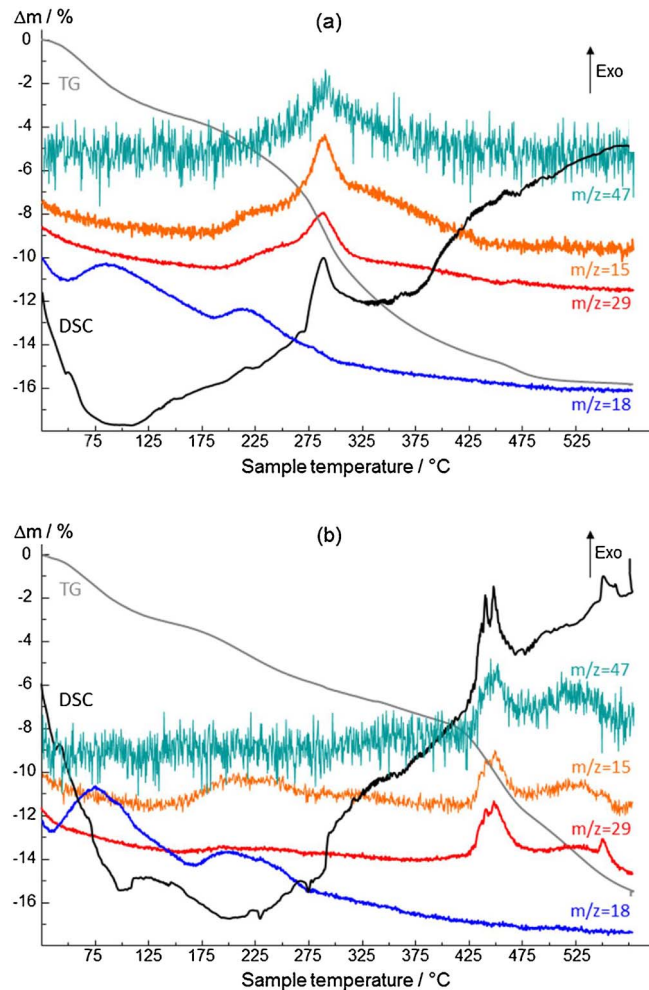


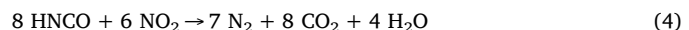
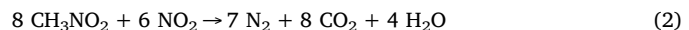
Fig. 10. TG, DSC curves, and MS profiles of ¹⁵N¹⁴N (m/z = 29)/¹⁵N (m/z = 15), H₂O (m/z = 18), and ¹⁵NO₂ (m/z = 47) measured on the impregnated 2.81 Co (a) and 0 Co (b) catalysts.

caused by the evolution of water. During the second TG step between 225–500 °C an exothermic effect at 288 °C is seen at which ¹⁵N¹⁴N (m/z = 29), ¹⁵N (m/z = 15), and ¹⁵NO₂ (m/z = 47) were detectable by MS analysis. This clearly indicates an exothermic reaction of ¹⁵NO₃⁻ with

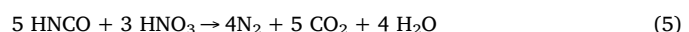
OCN⁻ in which ¹⁵N¹⁴N is formed already at 288 °C. The additionally evolved ¹⁵NO₂ might be stem from the decomposition of Na¹⁵NO₃ and can react with OCN⁻, too. Over the impregnated 0 Co catalyst ¹⁵N¹⁴N is formed at significant higher temperature around 450 °C (Fig. 10b) which leads in turn to the conclusion that the N₂ formation from the exothermic reaction of ¹⁵NO₃⁻ with OCN⁻ is catalyzed by Co.

Summarizing the results of the isotopic transient and TG-DSC-MS experiments it can be stated that isocyanate species are intermediates in the reduction of NO_y species by methane. This was confirmed by the quick isotopic exchange between Al³⁺–N¹²CO and Al³⁺–N¹³CO which proceeds faster than the formation of ¹³CO₂. Furthermore, it was proved by TG-DSC-MS investigation of 2.81 Co impregnated with Na¹⁵NO₃ and NaOCN that ¹⁵N¹⁴N is already formed at 288 °C by an exothermic reaction of ¹⁵NO₃⁻ with OCN⁻ catalyzed by Co.

It is obvious that isocyanate species are not directly formed by the interaction of CH₄ with NO_y species. It seems that nitromethane is the origin source which can conclude from studies of nitromethane interaction with Co-ZSM-5 catalysts [49,50]. Lombardo et al. [49] studied the reaction of nitromethane with NO, NO/O₂, and NO₂/O₂ over Co-ZSM-5 and found 100% conversion to N₂ at 500 °C in the case of NO/O₂ and NO₂/O₂, while the conversion in the case of CH₄/NO/O₂ was only 40% at the same temperature. When NO/O₂/CH₃NO₂ was substituted by the labeled feed ¹⁵NO/¹⁸O₂/CH₃NO₂ the predominant N₂ product was ¹⁵N¹⁴N, indicating that CH₃NO₂ and NO₂ contribute to N₂ formation (Eq. (2)). Furthermore, Cowan et al. [50] found that HNCO is the initial decomposition product of nitromethane which is adsorbed at catalyst surface and react with NO₂ to form N₂ (Eq. (3) and (4)).



These findings suggest that both, initially formed nitromethane and/or isocyanate species can react with NO₂. Our TG-DSC-MS investigations have shown that also preadsorbed nitrate species can react with isocyanate species (Eq. (5)).



However, under dynamic conditions and exposing the catalyst to the complete CH₄/NO/O₂ feed the reaction of primarily formed nitromethane and/or isocyanate with NO₂ seems to be preferred.

4. Conclusions

Comprehensive characterization data reveal that *i*) only a part of Co^{2+} is located at exchange positions independently from the Co content because Brønsted acidic sites were detected at all studied catalysts; *ii*) Co^{2+} is located at exchange positions as well as in oxide-like clusters located in the zeolite cavities; *iii*) all catalysts contain a remarkable percentage of Co^{3+} which is present in the oxide-like clusters as well as in Co_3O_4 and/or phyllosilicate phases; it can therefore be assumed that the oxide-like clusters contain Co^{2+} as well as Co^{3+} .

NO is oxidized by Co^{3+} species present in oxide-like clusters forming NO_2 and adsorbed NO_y species. Gaseous oxygen is required to reoxidize the formed Co^{2+} according a Mars-van-Krevelen mechanism and, thus, to establish an active $\text{Co}^{3+}/\text{Co}^{2+}$ redox pair. The isolated Co^{2+} cations located at exchange positions play an indirect role, facilitating chemisorption of NO and, thus, practically act as storage sites for NO.

The *operando* DRIFTS/UV-vis measurements reveal that pre-adsorbed NO_y species formed by oxidation of NO at Co^{3+} sites are reduced by gaseous CH_4 corresponding to an Eley-Rideal mechanism. As a consequence of this reaction N_2 is formed accompanied by water and CO_2 formation. Isocyanate species were identified as possible intermediates which can react with NO_y species or NO_2 to form N_2 . Thus, $^{15}\text{N}^{14}\text{N}$ formation at already 288 °C was observed by TG-DSC-MS investigation of 2.81 Co impregnated with $\text{Na}^{15}\text{NO}_3$ and NaOCN . This exothermic reaction of $^{15}\text{NO}_3^-$ with OCN^- is catalyzed by Co because on Co-free sample $^{15}\text{N}^{14}\text{N}$ formation was observed at significant higher temperature. It is likely that under dynamic conditions ($\text{CH}_4/\text{NO}/\text{O}_2$ feed) the reaction of primarily formed nitromethane and/or isocyanate with NO_2 is preferred.

Acknowledgments

The authors thank Christine Rautenberg for performing the pyridine and CO adsorption as well as the TG-DSC-MS experiments, Anja Simmula for the ICP-OES analysis, and Carsten Kreyenschulte for the TEM images. Furthermore, we would like to thank Udo Armbruster and Reinhard Eckelt for providing the test apparatus and technical support. Andrea Bellmann acknowledges financial support from the Leibniz-Gemeinschaft under the research grant SAW-2013-LIKAT-2.

Appendix A. Supplementary data

Supplementary material related to this article can be found, in the online version, at doi:<https://doi.org/10.1016/j.apcatb.2018.02.051>.

References

- [1] J.N. Armor, Catal. Today 26 (1995) 147–158.
- [2] Y. Tra, B. Burger, J. Weitkamp, Microporous Microporous Mater. 30 (1999) 3–41.
- [3] Y. Li, T. Slager, J.N. Armor, J. Catal. 150 (1994) 388–399.
- [4] D.B. Lukyanov, E.A. Lombardo, G.A. Sill, J.L. d'Itri, W.K. Hall, J. Catal. 163 (1996) 447–456.
- [5] T. Sun, M.D. Fokema, J.Y. Ying, Catal. Today 33 (1997) 251–261.
- [6] X. Wang, H.-Y. Chen, W.M.H. Sachtler, J. Catal. 197 (2001) 281–291.
- [7] A.D. Cowan, R. Dumpelmann, N.W. Cant, J. Catal. 151 (1995) 356–363.
- [8] E.M. Sadovskaya, A.P. Suknev, L.G. Pinaeva, V.B. Goncharov, B.S. Bal'zhinimaev,
- C. Chupin, C. Mirodatos, J. Catal. 201 (2001) 159–168.
- [9] E.M. Sadovskaya, A.P. Suknev, L.G. Pinaeva, V.B. Goncharov, B.S. Bal'zhinimaev, C. Chupin, J. Pérez-Ramírez, C. Mirodatos, J. Catal. 225 (2004) 179–189.
- [10] C. Chupin, A. Vanveen, M. Konduru, J. Despres, C. Mirodatos, J. Catal. 241 (2006) 103–114.
- [11] G. Busca, M.A. Larrubia, L. Arrighi, G. Ramis, Catal. Today 107–108 (2005) 139–148.
- [12] T. Montanari, O. Marie, M. Daturi, G. Busca, Catal. Today 110 (2005) 339–344.
- [13] T. Montanari, O. Marie, M. Daturi, G. Busca, Appl. Catal. B 71 (2007) 216–222.
- [14] B. Djonev, B. Tsintsarski, D. Klissurski, K. Hadjiivanov, J. Chem. Soc. Faraday Trans. 93 (1997) 4055–4063.
- [15] K. Hadjiivanov, B. Tsintsarski, T. Nikolova, Phys. Chem. Chem. Phys. 1 (1999) 4521–4528.
- [16] F. Lóny, H.E. Solt, Z. Pászti, J. Valyon, Appl. Catal. B 150–151 (2014) 218–229.
- [17] D. Kaucký, A. Vondrová, J. Dědeček, B. Wichterlová, J. Catal. 194 (2000) 318–329.
- [18] J. Dědeček, B. Wichterlová, J. Phys. Chem. B 103 (1999) 1462–1476.
- [19] D. Kaucký, J. Dědeček, B. Wichterlová, Microporous Microporous Mater. 31 (1999) 75–87.
- [20] J. Dědeček, D. Kaucký, B. Wichterlová, Microporous Microporous Mater. 35–36 (2000) 483–494.
- [21] M.C. Campa, S. De Rossi, G. Ferraris, V. Indovina, Appl. Catal. B 8 (1996) 315–331.
- [22] M.C. Campa, I. Luisetto, D. Pietrogiacomi, V. Indovina, Appl. Catal. B 46 (2003) 511–522.
- [23] D. Tibiletti, A. Goguet, D. Reid, F.C. Meunier, R. Burch, Catal. Today 113 (2006) 94–101.
- [24] R. Buzzoni, S. Bordiga, G. Ricchiardi, C. Lamberti, A. Zecchina, G. Bellussi, Langmuir 12 (1996) 930–940.
- [25] G. Busca, Phys. Chem. Chem. Phys. 1 (1999) 723–736.
- [26] D.J. Parrillo, D. Dolenc, R.J. Gorte, R.W. McCabe, J. Catal. 142 (1993) 708–718.
- [27] K. Góra-Marek, B. Gil, M. Śliwa, J. Datka, Appl. Catal. A 330 (2007) 33–42.
- [28] K. Góra-Marek, B. Gil, J. Datka, Appl. Catal. A 353 (2009) 117–122.
- [29] K. Góra-Marek, Top. Catal. 52 (2009) 1023–1029.
- [30] G. Bagnasco, M. Turco, C. Resini, T. Montanari, M. Bevilacqua, G. Busca, J. Catal. 225 (2004) 536–540.
- [31] L.M. Kustov, V.B. Kazansky, S. Beran, L. Kubelková, P. Jirů, J. Phys. Chem. 91 (1987) 5247–5251.
- [32] A. Zecchina, S. Bordiga, C. Lamberti, G. Spoto, L. Carnelli, C. Otero Areán, J. Phys. Chem. 98 (1994) 9577–9582.
- [33] K. Hadjiivanov, E. Ivanova, M. Daturi, J. Saussey, J.-C. Lavalle, Chem. Phys. Lett. 370 (2003) 712–718.
- [34] M. Lezcano, V.I. Kovalchuk, J.L. d'Itri, Kinet. Catal. 42 (2001) 104–111.
- [35] K. Hadjiivanov, Catal. Rev. Sci. Eng. 42 (2000) 71–144.
- [36] A.A. Verberckmoes, B.M. Weckhuysen, R.A. Schoonheydt, Microporous Mesoporous Mater. 22 (1998) 165–178.
- [37] B. Kraushaar-Czarnetzki, W.G.M. Hoogervorst, R.R. Andréa, C.A. Emeis, W.H.J. Stork, J. Chem. Soc. Faraday Trans. 87 (1991) 891–895.
- [38] X. Wang, H.-Y. Chen, W.M.H. Sachtler, Appl. Catal. B 26 (2000) L227–L239.
- [39] X. Wang, H. Chen, W.M.H. Sachtler, Appl. Catal. B 29 (2001) 47–60.
- [40] M. Mhamdi, E. Marceau, S. Khaddar-Zine, A. Ghorbel, M. Che, Y.B. Taarit, F. Villain, Catal. Lett. 98 (2004) 135–140.
- [41] C. Resini, T. Montanari, L. Nappi, G. Bagnasco, M. Turco, G. Busca, F. Bregani, M. Notaro, G. Rocchini, J. Catal. 214 (2003) 179–190.
- [42] H. Li, M. Rivalan, F. Thibault-Starzyk, A. Travert, F.C. Meunier, Phys. Chem. Chem. Phys. 15 (2013) 7321–7327.
- [43] F.C. Meunier, React. Chem. Eng. 1 (2016) 134–141.
- [44] F. Solymosi, T. Bánsági, J. Catal. 156 (1995) 75–84.
- [45] S.A. Beloshapkin, E.A. Paukshtis, V.A. Sadykov, J. Mol. Catal. A 158 (2000) 355–359.
- [46] L.J. Lobree, A.W. Aylor, J.A. Reimer, A.T. Bell, J. Catal. 169 (1997) 188–193.
- [47] S.-K. Park, H. Choo, L. Kevan, Phys. Chem. Chem. Phys. 3 (2001) 3247–3253.
- [48] A. Satsuma, A.D. Cowan, N.W. Cant, D.L. Trimm, J. Catal. 181 (1999) 165–169.
- [49] E.A. Lombardo, G.A. Sill, J.L. d'Itri, W.K. Hall, J. Catal. 173 (1998) 440–449.
- [50] A.D. Cowan, N.W. Cant, B.S. Haynes, P.F. Nelson, J. Catal. 176 (1998) 329–343.
- [51] V.A. Sadykov, V.V. Lunin, V.A. Matyshak, E.A. Paukshtis, A.Ya. Rozovskii, N.N. Bulgakov, J.R.H. Ross, Kinet. Catal. 44 (2003) 379–400.
- [52] T. Ataloglou, J. Vakros, K. Bourikas, C. Fountzoulas, C. Kordulis, A. Lycourghiotis, Appl. Catal. B 57 (2005) 299–321.
- [53] L.G.A. van de Water, G.L. Bezemer, J.A. Bergwerff, M. Versluijs-Helder, B.M. Weckhuysen, K.P. de Jong, J. Catal. 242 (2006) 287–298.
- [54] F.C. Meunier, Catalysis 22 (2010) 94–118.